Nidogens are new therapeutic targets for the prevention of tetanus

Authors: Kinga Bercsenyi[1,2], Nathalie Schmieg[1,2], J. Barney Bryson[2], Paola Caccin[3], Matthew Golding[1,§], Giuseppe Zanotti[3], Linda Greensmith[2], Roswitha Nischt[4] and Giampietro Schiavo[2,*]

Affiliations:

[1]Molecular Neuropathobiology Laboratory, Cancer Research UK London Research Institute, 44 Lincoln's Inn Fields, London, WC2A 3LY, UK;

[2]Sobell Department of Motor Neuroscience & Movement Disorders, UCL Institute of Neurology, University College London, WC1N 3BG London, UK;

[3]Department of Biomedical Sciences, University of Padua, Viale G. Colombo 3, 35131 Padova, Italy;

[4]Department of Dermatology, University of Cologne, Kerpener Strasse 62, 50937 Cologne, Germany

*Correspondence to: Prof. Giampietro Schiavo, Sobell Department of Motor Neuroscience & Movement Disorders, UCL Institute of Neurology, University College London, Queen Square, WC1N 3BG London, UK Phone: ++44 7918 738393, Fax: ++44 20 7813 3107; e-mail: giampietro.schiavo@ucl.ac.uk

Present address: §Centre for Microvascular Research, William Harvey Research Institute, Barts & The London School of Medicine and Dentistry, Queen Mary, University of London, London, UK

Abstract: Tetanus neurotoxin (TeNT) is one of the most poisonous substances on Earth and a major cause of neonatal death in non-vaccinated areas (*1*). TeNT targets the neuromuscular junction (NMJ) with high affinity, yet the nature of the TeNT receptor complex at the NMJ remains unknown (*2*). Here we show that nidogens (also known as entactins (*3*)) are highly enriched at the basement membrane of the NMJ and are essential for TeNT binding to motor neurons, where TeNT enters the central nervous system to exert its toxic effects. Inhibition of the TeNT-nidogen interaction using small nidogen-derived peptides or genetic ablation of nidogen-2 protects mice from TeNT-induced spastic paralysis. Our report is the first to demonstrate the direct involvement of a protein receptor for TeNT at the NMJ, paving the way for the development of novel therapeutics for the prevention of tetanus targeting this novel protein-protein interaction.

Main Text:

TeNT is formed by two subunits, which perform specific functions necessary for its toxicity. The heavy (H) chain mediates high-affinity binding and entry into neurons, whereas the light (L) chain causes synaptic silencing of inhibitory interneurons, which normally suppress motor neuron activity, thereby inducing spastic paralysis (*4*). After internalisation into motor neurons, the carboxy-terminal fragment of the H chain (H_CT) is sorted to signalling endosomes, which undergo axonal retrograde transport towards the motor neuron cell body (*5*). We have previously characterised the proteome of these organelles using H_CT-conjugated magnetic nanoparticles and mass spectrometry (*5*). This affinity isolation approach identified a list of proteins associated with signalling endosomes, some of which were predicted to be involved in the binding and/or internalisation of H_CT. We analyzed the sequences of these proteins for the presence of the tripeptide Tyr-Glu-Trp (YEW), which was previously shown to interact with the sialic acid binding site of H_CT (*6*) (R site), a region implicated in polysialogangliosides and acidic lipid binding (*6, 7*). In contrast, the corresponding region of BoNTs interacts with the synaptic proteins SV2A-C or synaptotagmin I/II (*8-14*), raising the possibility that this site of TeNT also binds to a protein receptor.

We selected candidates containing variants of the YEW peptide within the lumen of signalling endosomes, a localization topologically equivalent to the extracellular domain of these proteins when localized to the plasma membrane (Supplementary Data Table 1). A total of 35 nine-residue peptides containing the YEW motif or closely related sequences were tested for binding to H_CT using direct fluorescent binding, ELISA and *in vitro* pull down assays (Fig. 1A; Supplementary Fig. 1). The interacting peptides were then assessed for their ability to compete for H_CT binding on primary neurons. Peptide N1, which corresponds to a short sequence in nidogen-1, a basement membrane (BM) protein (Supplementary Data Table 1; Supplementary Fig. 2A), was selected for further analyses as it significantly reduced H_CT binding to motor neurons (Fig. 1C,D). The YEW-like motif of nidogen-1 (YQW) was responsible for this interaction since a mutant form of this peptide, in which the aromatic residues were replaced by alanines (AQA; $N1_{AA}$) failed to inhibit H_CT binding to motor neurons (Fig. 1C,D).

We then tested whether H_CT was capable of interacting directly with full-length nidogen-1. Incubation of immobilised HA-tagged H_CT with full-length nidogen-1 revealed that the two proteins bind directly under these experimental conditions (Fig. 1B, upper panel). Moreover, the N1 peptide plays a key role in this interaction since pre-incubating H_CT with an excess of this peptide, but not the $N1_{AA}$ mutant, abolishes this binding.

Mammals express two nidogen isoforms that play partially redundant roles in BM formation and maintenance (*15, 16*). Whilst nidogen-2 knockout (KO) mice do not display any overt phenotype, animals lacking nidogen-1 develop a progressive hindlimb paralysis, indicating a role for this protein in motor neuron survival (*17*). Interestingly, nidogen-2 contains a variant of the YEW peptide (WSY; N2; Supplementary Data Table 1), suggesting that both nidogen isoforms could bind H_CT. Accordingly, we found that recombinant nidogen-2 directly binds to H_CT and this interaction is blocked by the N2 peptide, but not by its alanine mutant (ASA; $N2_{AA}$)(Fig. 1B, lower panel and Supplementary Data Table 1).

Nidogens are tightly integrated within the BM, which renders them hard to access for exogenous ligands. To determine whether nidogens are the limiting factor for H_CT binding to motor neurons, we added soluble full-length nidogen-1 to cultured motor neurons together with H_CT. This resulted in a dramatic increase in surface-bound H_CT (Fig. 1C,D), suggesting that the addition of exogenous nidogen-1 increases the number of H_CT binding sites on the motor neuron surface. This effect is dependent upon the YEW-like motif of nidogen-1, since preincubation with the N1, but not the $N1_{AA}$ peptide prevents this effect (Fig. 1C,D).

Inspection of the domain structure of nidogens revealed that N1 and N2 peptides are present in the globular G_2 domain (Supplementary Fig. 2A). Molecular modelling (Supplementary Fig. 2B-D) reveals that the N1 peptide, both in isolation and within the intact G_2 domain, is able to dock to the R site of H_CT, where sialic acid, disialyllactose and the tri-peptide YEW, bind (*6*). Surprisingly, the molecular surface concealed by the N1 peptide-H_CT complex constitutes more than 40% of the total peptide surface (Supplementary Fig. 2C), suggesting that the binding, which is driven by the potential formation of five hydrogen bonds and other polar interactions (Supplementary Data Table 2), is very strong.

The G2 domain of nidogen-1 fits into a large crevice at the top of the trefoil domain of H_CT (Supplementary Fig. 2B), concealing 1,114 $Å^2$ and 1,106 $Å^2$ for H_CT and the G2 domain of nidogen-1, respectively. Complex formation is likely to be promoted by complementary electrostatic surfaces and several potential hydrogen bonds (Supplementary Data Table 3 and Supplementary Fig. 2D). Crucially, the association between H_CT and nidogen-1 is unlikely to interfere with the interaction between H_CT and polysialogangliosides, which is required for TeNT binding to the neuronal surface (*7, 18*). Thus, nidogens and polysialogangliosides have the potential to bind TeNT simultaneously, and thereby fulfil the requirements for the proposed dual receptor model (*19, 20*), which predicts the concurrent interaction of lipid and protein receptors to TeNT and BoNTs for their high-affinity binding to neuronal membranes.

To determine whether H_CT and nidogens co-localize at the specialised BM forming the synaptic cleft of the NMJ, we incubated freshly dissected *levator auris longus* (LAL) muscle firstly with H_CT, followed by an antibody against nidogen-2 (α-nidogen-2). Both nidogen-2 and H_CT displayed similar distributions at the NMJ, which closely resembled the staining pattern obtained with α-bungarotoxin (BTX), a presynaptic NMJ marker, suggesting that both nidogen-2 and H_CT accumulate at the synaptic cleft (Fig. 2A). We then asked whether these two proteins are internalised and transported together in signalling endosomes. H_CT and α-nidogen-2 were added to motor neurons at 37˚C and after a mild acid wash to remove all probes still bound to the neuronal surface, we immunostained for α-nidogen-2. The extensive co-localization between α-nidogen-2 and H_CT along the axon strongly indicated that these two proteins were internalised and transported by the same organelles (Fig. 2B). Furthermore, co-immunoprecipitation of H_CT and endogenous nidogen-2 from motor neurons incubated with H_CT for 5 minutes at 37˚C (Fig. 2C) suggested that this interaction is preserved upon entry of H_CT into endosomal compartments.

After axonal transport to the cell body, TeNT undergoes transcytosis and re-uptake into spinal interneurons, where it blocks the release of inhibitory neurotransmitters, leading

to the characteristic symptoms of clinical tetanus (*4*). To address whether nidogens are targeted together with H_CT to the plasma membrane of soma and dendrites following axonal transport, motor neurons were plated into microfluidic chambers (*21*) and co-incubated with fluorescent H_CT and α-nidogen-2 in the axonal compartment (AX; Supplementary Fig. 3A) for 2 h at 37˚C. The somal side (CB; Supplementary Fig. 3A) of these chambers was then immunostained in non-permeabilizing conditions to determine whether H_CT and nidogen-2 were subsequently re-exposed onto the plasma membrane. This was indeed the case, as shown by the co-localization of the two probes as distinct punctae on the motor neuron surface (Supplementary Fig. 3B). This observation suggests that the nidogen-H_CT complex persists all along the intracellular trafficking route connecting the NMJ to the spinal cord and may facilitate the transcytosis of TeNT into inhibitory interneurons (*4*), thus clarifying the mechanism by which TeNT targets these neurons to exert its toxic function.

To further test the importance of nidogens in TeNT intoxication, we assessed the ability of H_CT to bind nidogen KO neurons and tissue, and determined the susceptibility of nidogen KO mice to TeNT-induced paralysis. We observed a significant decrease in the amount of H_CT bound to nidogen-2 KO motor neurons compared to wild type neurons (Fig. 3A,B). Next, we tested whether the NMJ uptake of H_CT was impaired in mice lacking nidogens. For this purpose, isolated LAL muscles were incubated with HA-H_CT and immunostained for HA, which revealed a dramatic reduction in the ability of NMJs from both nidogen-1 and nidogen-2 KO mice to bind and internalise H_CT (Fig. 3C,D). Nidogen-1 and -2 double knockout (DKO) animals show early embryonic lethality (*22*), precluding the derivation of motor neuron cultures from these mice. To overcome this limitation, we assayed H_CT uptake in hindbrains of DKO embryos at E11.5. Whilst control hindbrains displayed robust H_CT staining (Fig. 3E, left), hindbrains from DKO littermates were unable to bind H_CT, indicating that nidogen-1 and -2 are essential for H_CT binding *in vivo* (Fig. 3E,F).

Having identified nidogens as novel H_CT co-receptors, we next investigated the ability of the N1 peptide to prevent uptake of TeNT *in vivo*, using three independent assays. Firstly, full length TeNT was injected locally into the *triceps surae* muscle either alone, or in combination with N1 or $N1_{AA}$ and the effect on spastic paralysis was assessed using footprint analysis 24 h after injection (Fig. 4A,B). TeNT caused a permanent plantar-flexion of the affected hind-paw (Supplementary Movie 1) and severe gait abnormalities, with the characteristic inability to place the affected hind-paw in the former position of the ipsilateral fore-paw, as occurs in normal mice (Fig. 4A,B). Strikingly, co-administration of the N1 peptide completely abolished these TeNT-induced gait abnormalities (Supplementary Movie 1), whereas the $N1_{AA}$ peptide was ineffective (Fig. 4A,B).

To corroborate this finding, we quantified the protective effect of the N1 peptide co-injected with TeNT on the TeNT-induced spastic paralysis by measuring the maximal force generated by the *tibialis anterior* muscle using isometric muscle tension physiology. The contractile force of the TeNT-injected muscle was diminished (3.11±0.88% of non-injected control)(Fig. 4C, Supplementary Fig. 4A), as was the case with muscles co-injected with TeNT and the $N1_{AA}$ peptide (2.14±1.44% of non-injected control)(Fig. 4C, Supplementary Fig. 4B). Co-administration of the N1 peptide reduced the TeNT-mediated decline in contractile force compared to the other two groups (47.46 ±10.31% of non-injected

control)(Fig. 4C, Supplementary Fig. 4C). Similar results were obtained using phrenic nerve-hemidiaphragm preparations (*23*) (Supplementary Fig. 4D). Together, these results confirm the ability of the N1 peptide to prevent symptoms of tetanus *in vivo*.

Next, we injected wild type and nidogen-2 KO mice intraperitoneally with different doses of TeNT and closely monitored the appearance of the hallmark symptoms of tetanus. Nidogen-2 KO animals showed a significant delay in the onset and progression of tetanic symptoms at lower TeNT doses (Fig. 4D). Unfortunately, the possibility to extend these assays to mice lacking nidogen-1 was precluded by the severe epileptic and paralytic phenotype affecting these animals (*17*).

Interestingly, some of the symptoms observed in nidogen-2 KO mice injected with TeNT, such as *keratoconjuctivitis sicca* (*24*) (data not shown), resembled those of botulism, suggesting that in the absence of one of its physiological receptors, a proportion of TeNT may exploit an alternative route of entry at the NMJ, which is shared with BoNTs. Cross talk between the two modes of entry and intracellular transport pathways of TeNT and BoNT has been previously suggested (*21*), and is supported by the botulism-like symptoms shown by mice injected with high doses of TeNT (*25*).

Since BoNTs use several SV2 isoforms as receptors (*12-14, 23*) and SV2A has been proposed as TeNT receptor in inhibitory neurons (*26*), we quantified the co-localization of H_CT with SV2A and C in motor neurons and tested if pre-incubation of H_CT with recombinant nidogen-1 altered this process. SV2A showed robust co-localization with H_CT internalised for 45 min at 37 °C (45%; Fig. 4E,F), whereas the co-distribution of H_CT with SV2C was negligible (Supplementary Fig. 4C,D). This result suggests that at least a sub-pool of TeNT could be internalised via synaptic vesicle recycling at the relatively high concentrations of H_CT used in our binding assay (40 nM). However, the addition of recombinant nidogen-1 caused a significant reduction in the co-localization between H_CT and SV2A (Fig. 4E,F) but not SV2C (Supplementary Fig. 4E,F). This decrease is due to the dramatic increase of the pool of H_CT accumulated in the soma (Fig. 4E), suggesting that in the presence of exogenous nidogens, H_CT is preferentially targeted to an endocytic pathway linked to axonal retrograde transport and avoids the synaptic vesicle recycling route.

In conclusion, we have identified the long-awaited protein receptor for TeNT at the NMJ as well as a potential mechanism to explain the overlap between the entry routes of TeNT and BoNT (Supplementary Fig. 5). Interestingly, engineered growth factors with higher affinity for the extracellular matrix display enhanced biological activity (*27*), indicating that this process is crucial for their signalling and biological function (*28*). TeNT might exploit a similar strategy based on a very efficient capture mechanism at specialised NMJ sites, which could concentrate TeNT as well as physiological ligands, such as neurotrophic factors, for their uptake and sorting to transport organelles. This physiological pathway is likely to be indispensable to the host cell, enabling TeNT to be so deadly at such low concentrations. Understanding this mechanism at a molecular level is therefore crucial to refine the biological properties of bioactive peptides for their use in human therapy, and to develop specific molecules altering the capture of this powerful toxin at the NMJ, thus blocking its CNS effects.

References and Notes:

1. WHO, Global Immunization Data. (2014); published online Epub02.2014 (http://www.who.int/immunization/monitoring_surveillance/Global_Immunization_Data.pdf?ua=1).
2. C. Montecucco, O. Rossetto, G. Schiavo, Presynaptic receptor arrays for clostridial neurotoxins. *Trends Microbiol.* **12**, 442-446 (2004); published online EpubOct (10.1016/j.tim.2004.08.002).
3. B. Carlin, R. Jaffe, B. Bender, A. E. Chung, Entactin, a novel basal lamina-associated sulfated glycoprotein. *J. Biol. Chem.* **256**, 5209-5214 (1981); published online EpubMay 25 (
4. C. Montecucco, Clostridial Neurotoxins: The Molecular Pathogenesis of Tetanus and Botulism *Curr. Top. Microbiol. Immunol.* **195**, 278 (1995).
5. K. Deinhardt, S. Salinas, C. Verastegui, R. Watson, D. Worth, S. Hanrahan, C. Bucci, G. Schiavo, Rab5 and Rab7 control endocytic sorting along the axonal retrograde transport pathway. *Neuron* **52**, 293-305 (2006); published online EpubOct 19 (S0896-6273(06)00640-4 [pii] 10.1016/j.neuron.2006.08.018).
6. S. Jayaraman, S. Eswaramoorthy, D. Kumaran, S. Swaminathan, Common binding site for disialyllactose and tri-peptide in C-fragment of tetanus neurotoxin. *Proteins* **61**, 288-295 (2005); published online EpubNov 1 (10.1002/prot.20595).
7. C. Chen, Z. J. Fu, J. J. P. Kim, J. T. Barbieri, M. R. Baldwin, Gangliosides as High Affinity Receptors for Tetanus Neurotoxin. *J. Biol. Chem.* **284**, 26569-26577 (2009); published online EpubSep 25 (Doi 10.1074/Jbc.M109.027391).
8. Q. Chai, J. W. Arndt, M. Dong, W. H. Tepp, E. A. Johnson, E. R. Chapman, R. C. Stevens, Structural basis of cell surface receptor recognition by botulinum neurotoxin B. *Nature* **444**, 1096-1100 (2006); published online EpubDec 21 (10.1038/nature05411).
9. R. Jin, A. Rummel, T. Binz, A. T. Brunger, Botulinum neurotoxin B recognizes its protein receptor with high affinity and specificity. *Nature* **444**, 1092-1095 (2006); published online EpubDec 21 (10.1038/nature05387).
10. R. P. A. Berntsson, L. S. Peng, L. M. Svensson, M. Dong, P. Stenmark, Crystal Structures of Botulinum Neurotoxin DC in Complex with Its Protein Receptors Synaptotagmin I and II. *Structure* **21**, 1602-1611 (2013); published online EpubSep 3 (Doi 10.1016/J.Str.2013.06.026).
11. R. P. A. Berntsson, L. S. Peng, M. Dong, P. Stenmark, Structure of dual receptor binding to botulinum neurotoxin B. *Nature Communications* **4**, (2013); published online EpubJun (Artn 2058 Doi 10.1038/Ncomms3058).
12. M. Dong, F. Yeh, W. H. Tepp, C. Dean, E. A. Johnson, R. Janz, E. R. Chapman, SV2 is the protein receptor for botulinum neurotoxin A. *Science* **312**, 592-596 (2006); published online EpubApr 28 (10.1126/science.1123654).
13. L. Peng, W. H. Tepp, E. A. Johnson, M. Dong, Botulinum neurotoxin D uses synaptic vesicle protein SV2 and gangliosides as receptors. *PLoS Pathog.* **7**, e1002008 (2011); published online EpubMar (10.1371/journal.ppat.1002008).
14. R. M. Benoit, D. Frey, M. Hilbert, J. T. Kevenaar, M. M. Wieser, C. U. Stirnimann, D. McMillan, T. Ceska, F. Lebon, R. Jaussi, M. O. Steinmetz, G. F. Schertler, C. C. Hoogenraad, G. Capitani, R. A. Kammerer, Structural basis for recognition of

synaptic vesicle protein 2C by botulinum neurotoxin A. *Nature* **505**, 108-111 (2014); published online EpubJan 2 (10.1038/nature12732).

15. K. Mann, R. Deutzmann, M. Aumailley, R. Timpl, L. Raimondi, Y. Yamada, T. C. Pan, D. Conway, M. L. Chu, Amino acid sequence of mouse nidogen, a multidomain basement membrane protein with binding activity for laminin, collagen IV and cells. *EMBO J.* **8**, 65-72 (1989); published online EpubJan (
16. M. S. Ho, K. Bose, S. Mokkapati, R. Nischt, N. Smyth, Nidogens-Extracellular matrix linker molecules. *Microsc. Res. Tech.* **71**, 387-395 (2008); published online EpubMay (10.1002/jemt.20567).
17. L. Dong, Y. Chen, M. Lewis, J. C. Hsieh, J. Reing, J. R. Chaillet, C. Y. Howell, M. Melhem, S. Inoue, J. R. Kuszak, K. DeGeest, A. E. Chung, Neurologic defects and selective disruption of basement membranes in mice lacking entactin-1/nidogen-1. *Lab. Invest.* **82**, 1617-1630 (2002); published online EpubDec (
18. T. Binz, A. Rummel, Cell entry strategy of clostridial neurotoxins. *J. Neurochem.* **109**, 1584-1595 (2009); published online EpubJun (10.1111/j.1471-4159.2009.06093.x).
19. C. Montecucco, How do tetanus and botulinum neurotoxins bind to neuronal membranes? *Trends Biochem. Sci.* **11**, 315-317 (1986).
20. A. Rummel, T. Eichner, T. Weil, T. Karnath, A. Gutcaits, S. Mahrhold, K. Sandhoff, R. L. Proia, K. R. Acharya, H. Bigalke, T. Binz, Identification of the protein receptor binding site of botulinum neurotoxins B and G proves the double-receptor concept. *Proc. Natl. Acad. Sci. U. S. A.* **104**, 359-364 (2007); published online EpubJan 2 (10.1073/pnas.0609713104).
21. L. Restani, F. Giribaldi, M. Manich, K. Bercsenyi, G. Menendez, O. Rossetto, M. Caleo, G. Schiavo, Botulinum neurotoxins A and E undergo retrograde axonal transport in primary motor neurons. *PLoS Pathog.* **8**, e1003087 (2012); published online EpubDec (10.1371/journal.ppat.1003087).
22. B. L. Bader, N. Smyth, S. Nedbal, N. Miosge, A. Baranowsky, S. Mokkapati, M. Murshed, R. Nischt, Compound genetic ablation of nidogen 1 and 2 causes basement membrane defects and perinatal lethality in mice. *Mol. Cell. Biol.* **25**, 6846-6856 (2005); published online EpubAug (10.1128/MCB.25.15.6846-6856.2005).
23. S. Mahrhold, A. Rummel, H. Bigalke, B. Davletov, T. Binz, The synaptic vesicle protein 2C mediates the uptake of botulinum neurotoxin A into phrenic nerves. *FEBS Lett.* **580**, 2011-2014 (2006); published online EpubApr 3 (10.1016/j.febslet.2006.02.074).
24. O. Suwan-apichon, M. Rizen, R. Rangsin, S. Herretes, J. M. Reyes, K. Lekhanont, R. S. Chuck, Botulinum toxin B-induced mouse model of keratoconjunctivitis sicca. *Invest. Ophthalmol. Vis. Sci.* **47**, 133-139 (2006); published online EpubJan (10.1167/iovs.05-0380).
25. M. Matsuda, N. Sugimoto, K. Ozutsumi, T. Hirai, Acute botulinum-like intoxication by tetanus neurotoxin in mice. *Biochem. Biophys. Res. Commun.* **104**, 799-805 (1982); published online EpubJan 29 (
26. F. L. Yeh, M. Dong, J. Yao, W. H. Tepp, G. Lin, E. A. Johnson, E. R. Chapman, SV2 mediates entry of tetanus neurotoxin into central neurons. *PLoS Pathog.* **6**, e1001207 (2010)10.1371/journal.ppat.1001207).

27. M. M. Martino, P. S. Briquez, E. Guc, F. Tortelli, W. W. Kilarski, S. Metzger, J. J. Rice, G. A. Kuhn, R. Muller, M. A. Swartz, J. A. Hubbell, Growth factors engineered for super-affinity to the extracellular matrix enhance tissue healing. *Science* **343**, 885-888 (2014); published online EpubFeb 21 (10.1126/science.1247663).
28. L. Macri, D. Silverstein, R. A. Clark, Growth factor binding to the pericellular matrix and its importance in tissue engineering. *Adv Drug Deliv Rev* **59**, 1366-1381 (2007); published online EpubNov 10 (10.1016/j.addr.2007.08.015).
29. S. Bohnert, G. Schiavo, Tetanus toxin is transported in a novel neuronal compartment characterized by a specialized pH regulation. *J. Biol. Chem.* **280**, 42336-42344 (2005); published online EpubDec 23 (10.1074/jbc.M506750200).
30. P. Emsley, K. Cowtan, Coot: model-building tools for molecular graphics. *Acta Crystallogr. D Biol. Crystallogr.* **60**, 2126-2132 (2004); published online EpubDec (10.1107/S0907444904019158).
31. A. T. Brunger, Version 1.2 of the Crystallography and NMR system. *Nat. Protoc.* **2**, 2728-2733 (2007)10.1038/nprot.2007.406).
32. K. Arnold, L. Bordoli, J. Kopp, T. Schwede, The SWISS-MODEL workspace: a web-based environment for protein structure homology modelling. *Bioinformatics* **22**, 195-201 (2006); published online EpubJan 15 (10.1093/bioinformatics/bti770).
33. M. Kvansakul, M. Hopf, A. Ries, R. Timpl, E. Hohenester, Structural basis for the high-affinity interaction of nidogen-1 with immunoglobulin-like domain 3 of perlecan. *EMBO J.* **20**, 5342-5346 (2001); published online EpubOct 1 (10.1093/emboj/20.19.5342).
34. R. J. Carter, L. A. Lione, T. Humby, L. Mangiarini, A. Mahal, G. P. Bates, S. B. Dunnett, A. J. Morton, Characterization of progressive motor deficits in mice transgenic for the human Huntington's disease mutation. *J. Neurosci.* **19**, 3248-3257 (1999); published online EpubApr 15 (
35. J. B. Bryson, C. Hobbs, M. J. Parsons, K. D. Bosch, A. Pandraud, F. S. Walsh, P. Doherty, L. Greensmith, Amyloid precursor protein (APP) contributes to pathology in the SOD1(G93A) mouse model of amyotrophic lateral sclerosis. *Hum. Mol. Genet.* **21**, 3871-3882 (2012); published online EpubSep 1 (10.1093/hmg/dds215).
36. M. Hopf, W. Gohring, A. Ries, R. Timpl, E. Hohenester, Crystal structure and mutational analysis of a perlecan-binding fragment of nidogen-1. *Nat. Struct. Biol.* **8**, 634-640 (2001); published online EpubJul (10.1038/89683).

Acknowledgements: We thank S. Kjaer (Cancer Research UK London Research Institute) for help with the Octet RED96 system, K_D determination and data analysis, Subramanyam Swaminathan (Brookhaven National Laboratory) for experiments aiming at the crystallization of the N1 peptide-H_CT complex and Isabell Koxholt University of Cologne) for help with nidogen-1 and -2 KO mice. We also thank members of the Molecular Neuropathobiology Laboratory for constructive comments. This work was supported by Cancer Research UK (KB, NS, MG and GS), by the University of Padua (PC and GZ), and by the Deutsche Forschungsgemeinschaft (SFB 829) at the University of Cologne and the "Köln Fortune Programme" (RN). LG is a Graham Watts Senior Research Fellow, supported by the Brain Research Trust.

Authors' contribution: KB and GS were involved in study conception and design. KB, NS and GS carried out the biochemical, cell biology and toxicity experiments. JBB performed the physiology experiment on TA muscles. PC performed the phrenic nerve/hemidiaphragm intoxication experiments. GZ was responsible of the structural modelling. KB, NS, PC, JBB, MG, LG and GS interpreted the data. RN provided the nidogen-1 and -2 KO models and contributed to the discussion about nidogen function. KB and GS drafted the manuscript, whilst all authors contributed to its critical revision and approved the final version.

Conflict of interest

The authors declare that they have no conflict of interest.

Supplementary Information and Information on materials and methods is available on Science Online.

Figures

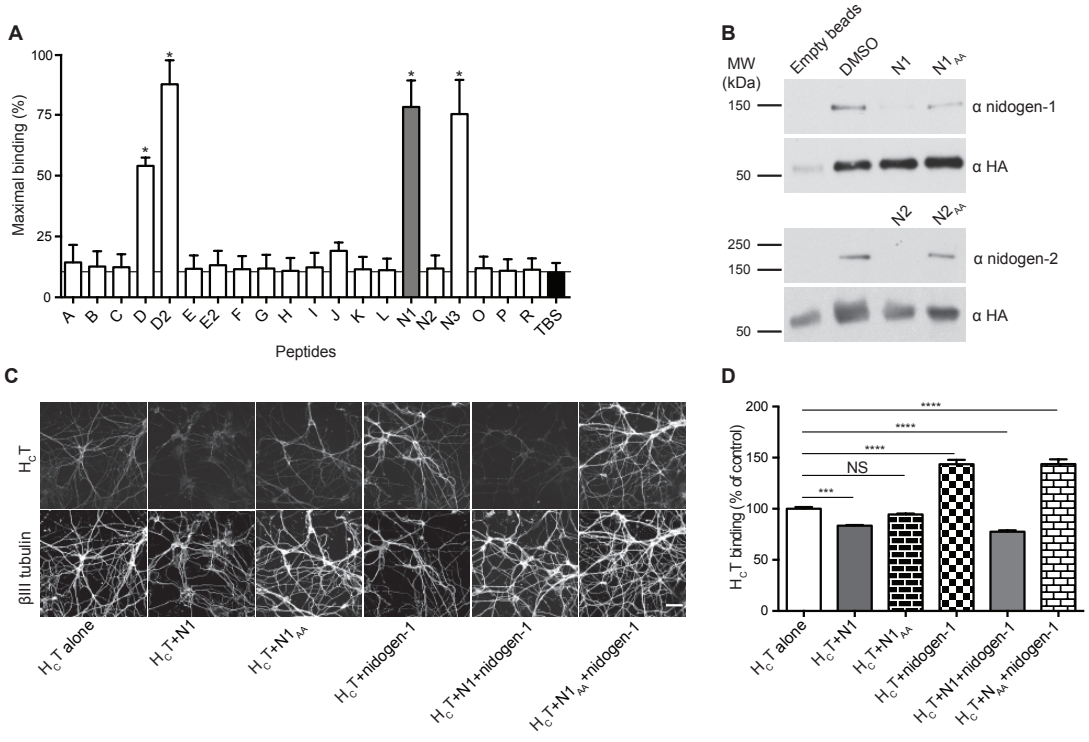

Fig. 1. **Nidogen peptides bind to H_CT and prevent its interaction with full-length nidogens *in vitro*. (A)** *In vitro* screen for peptides that bind fluorescent H_CT. The percentage of maximal binding was plotted for each peptide. The results were analyzed with paired t test between the individual peptides and Tris-buffered saline (TBS) controls (n=3; *, $p<0.05$; error bar: SD). **(B)** In vitro pull down of HA-H_CT preincubated with full length nidogen-1 (upper panel) or nidogen-2 (lower panel) with a mouse monoclonal anti-

HA antibody followed by SDS-PAGE and western blotting with rabbit anti-nidogen-1, rabbit anti-nidogen-2 or rat anti-HA antibodies. 'Empty beads' corresponds to samples in which HA-H_CT was omitted, and DMSO to samples treated with vehicle control. Both nidogen-1 and -2 bind directly to HA-H_CT, and pre-treatment with the N1 or N2 peptide blocks this interaction. In contrast, mutant peptides in which both the Y and W residues have been replaced by alanines ($N1_{AA}$ and $N2_{AA}$, respectively) are ineffective (*n*=3 for both proteins). **(C)** Motor neurons were incubated with AlexaFluor555-H_CT preincubated with vehicle control (H_CT alone) or wild type and mutant versions of the N1 peptide in the absence or the presence of exogenous nidogen-1 before staining for βIII tubulin and confocal imaging. Scale bar, 50 µm. **(D)** Twenty images were taken for each condition and fluorescence intensity of AlexaFluor555-H_CT bound to neurons (βIII tubulin mask) was quantified. Results were tested for statistical significance using one-way ANOVA followed by Dunnett's Multiple Comparison Test (*n*=3; NS, non significant; ***, p<0.005; ****, p<0.001; error bar: SD).

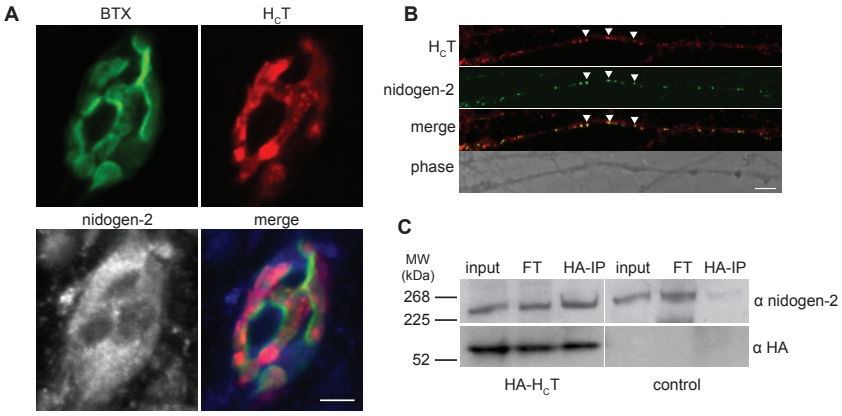

Fig. 2. Nidogen-2 co-localizes with H_CT at the neuromuscular junction and in primary motor neurons. (A) Whole mounts of *levator auris longus* (LAL) muscle were incubated with HA-H_CT and an antibody against nidogen-2. Neuromuscular junctions (NMJs) were labelled with AlexaFluor555-α-bungarotoxin (BTX, in green). H_CT (in red) binds to the NMJ at sites where nidogen-2 accumulates (grey). Scale bar, 5 µm, *n*=3. **(B)** Primary motor neurons were incubated with AlexaFluor555-H_CT and a rabbit anti-nidogen-2 antibody. Cells were acid washed, fixed and stained with an anti-rabbit IgG antibody. Scale bar, 5 µm (*n*=3). **(C)** Primary motor neurons were incubated with HA-H_CT for 5 min at 37˚C to allow binding and endocytosis. Since the binding of H_CT is detergent-sensitive, to preserve these interactions cells were pre-treated with a protein cross-linker (BSOCOES) before cell lysis. Nidogen-2 was immunoprecipitated from motor neuron lysates using an anti-HA antibody. In control samples, HA-H_CT was omitted (*n*=3).

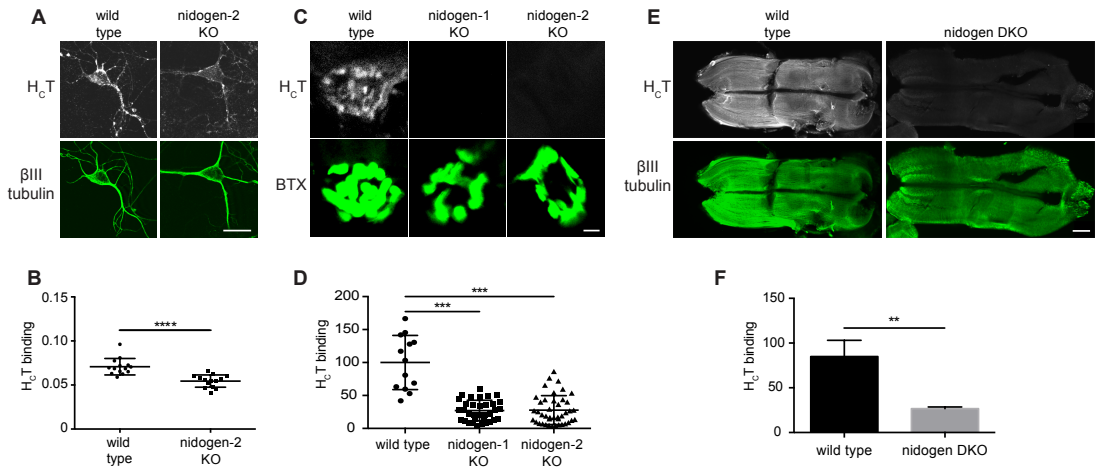

Fig. 3. Neurons lacking nidogens display reduced binding to H_CT. **(A)** Motor neurons derived from E13.5 wild type and nidogen-2 knockout (KO) embryos were incubated with AlexaFluor555-H_CT (grey). Cells were fixed and fluorescence intensity was measured in 10 images using a βIII tubulin mask (in green). **(B)** Results were plotted and analyzed using an unpaired t test with Welch's correction (*n*=3; ***, p<0.005; error bar: SD). (**C**) *Levator auris longus* (LAL) muscles of wild type, nidogen-1 and -2 KO animals were incubated with HA-H_CT, fixed and stained for HA (grey) and AlexaFluor555-α-bungarotoxin (BTX, in green) to identify neuromuscular junctions (NMJs). (**D**) Both nidogen-1 and -2 KO NMJs show a significant decrease in their ability to bind and internalise H_CT (one-way ANOVA followed by Dunnett's Multiple Comparison Test; *n*=3 animals per group, 20 images per animal; ***, p<0.005; error bar: SD). **(E)** Nidogen-1 and -2 double KO (DKO) and wild type E11.5 embryonic hindbrains were tested for H_CT binding and uptake. **(F)** Mean intensity of H_CT staining was measured and analyzed for significance using unpaired t test (*n*=3 animals per group; **, p<0.01; error bar: SD).

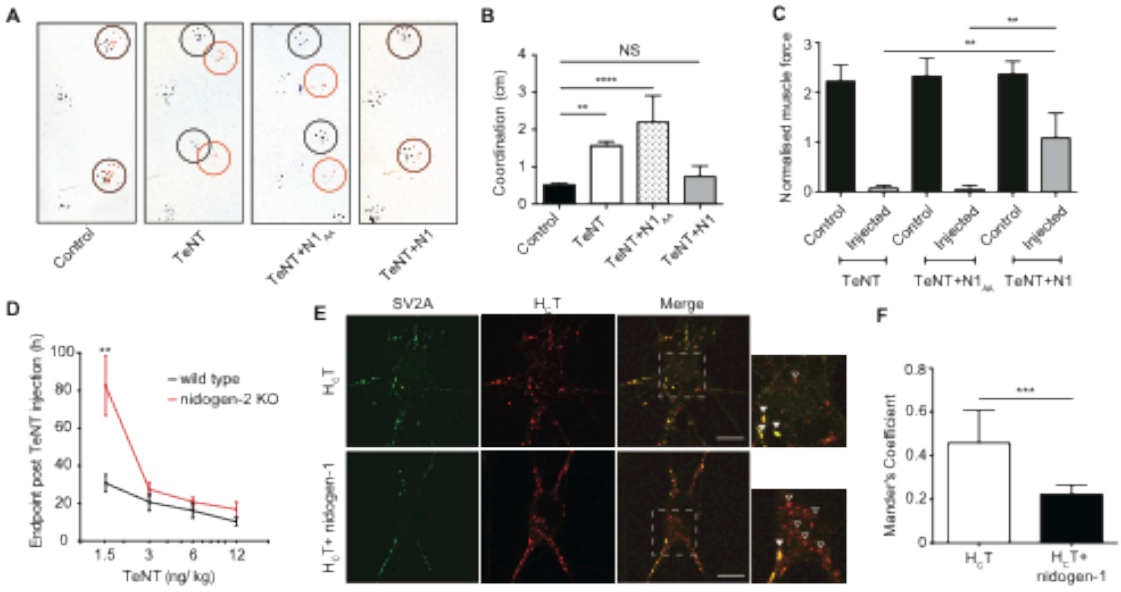

Fig. 4. The N1 peptide blocks tetanic paralysis and mice lacking nidogen-2 are less sensitive to TeNT. (A) Footprint analysis of control mice, or mice following injection into the gastrocnemius muscle of a sub-lethal dose of TeNT, or the same amount of TeNT preincubated with the $N1_{AA}$ or N1 peptides. The black circles show the non-injected paw prints; while the red circles mark the right hind paw (injected leg) prints. In control and TeNT+N1 mice, the black and red circles overlap, whilst in TeNT and TeNT+$N1_{AA}$ mice they are separated, indicating impairment in coordination due to local tetanus. **(B)** The distance between the paw prints on the injected side was measured and plotted to allow testing for statistical significance using one-way ANOVA followed by Dunnett's Multiple Comparison Test (*n*=2, 2 animals per group; NS, non significant; **, $p<0.01$; ****, $p<0.001$; error bar: SD). (**C)** The *tibialis anterior* (TA) muscle was injected with TeNT preincubated with either DMSO (vehicle control), $N1_{AA}$ or N1 peptides. Following anaesthesia, the tendon of the TA muscle was attached to a tension sensor and the peroneal nerve was stimulated. Maximal muscle force was measured, normalized to muscle weight and tested for significance (control vs. injected muscle). The N1-treated group retained a significantly higher muscle force than the vehicle- or $N1_{AA}$-treated groups. Significance was assessed by unpaired t test with Welch's correction (*n*=6 mice per group; **, $p<0.01$; error bar: SD). (**D)** Age and weight matched nidogen-2 KO and wild type mice were injected intraperitoneally with increasing doses of TeNT and monitored for up to 96 h. Animals were terminated at the loss of righting reflex and the time of termination was plotted against the dose of TeNT. Generalised tetanus in nidogen-2 KO animals is significantly delayed at lower doses (2 ng/kg) compared to wild type controls (*n*=2 experiments, minimum 2 mice per group; t test; ***, $p<0.005$; error bar: SD). **(E)** Wild type primary motor neurons were incubated either with AlexaFluor555-H_CT (shown in red; 40 nM) alone, or with AlexaFluor555-H_CT and recombinant full-length nidogen-1 (1.3 nM). Cells were fixed and stained for SV2A (in green) and βIII tubulin (not shown). **(F)** Mander's coefficient was used as an indicator of co-localization. Significance was assessed by unpaired t test (*n*=3, 10 images per condition; NS, non significant; ***, $p<0.005$; error bar: SD). Scale bar, 10 μm.

Supplementary Materials:

Materials and Methods:

Ethics statement

All experiments were carried out following the guidelines of the Cancer Research UK and UCL-Institute of Neurology genetic manipulation and Ethic Committees and in accordance with the European Community Council Directive of November 24, 1986 (86/609/EEC). Animal work was carried out under licence from the UK Home Office in accordance with the Animals (Scientific Procedures) Act 1986.

Reagents

All reagents were obtained from Sigma, unless stated otherwise. AlexaFluor-maleimide and AlexaFluor-conjugated antibodies were purchased from Life Technologies. Recombinant nidogens were purchased from R&D Systems. H_CT (441 residues) with an improved cysteine-rich tag was prepared as previously described (*29*) and labelled with

AlexaFluor555-maleimide following manufacturer's instructions, prior to dialysis against HEPES-NaOH 10 mM pH 7.4, 150 mM NaCl.

***In vitro* binding assays**

To screen peptides for H_CT binding, we dried 10 ng of biotin-labelled peptides on a 96-well plate overnight and incubated with Tris-buffered saline (TBS) containing 0.05% Tween and 1% bovine serum albumin (BSA) for 1 h to block unspecific interactions. Plates were then washed with TBS containing 0.05% Tween (TBST) three times before adding 40 nM AlexaFluor555-H_CT in TBS and incubating it overnight at 4°C. Plates were then extensively washed with TBS and the fluorescent signal was measured using an EnVision® Multilabel Plate Reader.

For classic ELISA, 96-well plates were prepared as before, washed with TBST three times before adding 4 nM VSVG-H_CT in TBS and then incubated overnight at 4°C. Wells were extensively washed with TBS and incubated with a monoclonal mouse antibody against VSVG (clone P5D4, Cancer Research UK; 1:500 in TBST) for 2 h at room temperature. Following washes with TBST, an HRP conjugated goat anti-mouse secondary antibody (1:2,000) was added for 1 h at room temperature. Wells were then washed with TBST and blocked with TBST+1% BSA before adding ortho-phenylenediamine (OPD) for 20 min. The reaction was stopped with 2 M HCl and absorbance at 490 nm was measured. Results were analyzed using unpaired t test.

For the *in vitro* immunoprecipitation assay, the biotin-tagged peptides (20 nM) were bound to streptavidine-coated agarose beads, and used to test the binding between the peptides and VSVG-H_CT. We added 1 mg VSVG-H_CT to the beads, and after extensive washes in TBS, samples were treated with Laemmli sample buffer, analyzed by SDS-PAGE and western blotting using the P5D4 anti-mouse monoclonal antibody. The intensity of the bands was measured in Image J and the results were analyzed by paired t test comparing the peptide bound beads to the empty bead control.

For the *in vitro* pull down assay, we bound HA-H_CT (1 mg) to α-HA (2 mg) coupled magnetic Dynabeads® (10 ml; Life Technologies). After blocking with 0.1 mg/ml BSA in phosphate buffered saline (PBS) for 1 h, samples were incubated with peptides (24 μM) or DMSO for 1 h at room temperature, washed and recombinant nidogens (0.5 mg of nidogen-1 or 1 mg of nidogen-2) were added to bind overnight at 4°C. Beads were then washed with PBS and bound proteins solubilised using Laemmli sample buffer prior to SDS-PAGE and immunoblotting using rabbit anti nidogen-1 and nidogen-2 (Abcam, ab14511 and ab14513 respectively; 1:500) and rat anti HA (3F10, Roche; 1:1000) antibodies.

For the cell-based endogenous immunoprecipitation, HA-H_CT (80 nM) was added to primary motor neurons for 5 min at 37 °C to allow endocytosis. The cells were immediately cooled on ice, washed with ice-cold Hank's buffer and proteins were cross-linked using BSOCOES (1 mM; Thermo Scientific) in PBS for 30 min at 4°C. The reaction was stopped by the addition of 50 mM Tris-HCl pH 7.5 (final concentration). Following washes with PBS, cells were lysed on ice using IP lysis buffer (20 mM Tris-HCl, 137 mM NaCl, 1 mM EDTA, 10% glycerol, 0.5% NP40, HALT protease inhibitors (Thermo Scientific)). The lysates were cleared by centrifugation and proteins binding to empty beads were cleared by incubating the samples with empty Dynabeads for 30 min at room temperature. Monoclonal mouse anti-HA antibody (12CA5; Cancer Research UK; 2 μg)

was cross-linked to Dynabeads (20 µl; Invitrogen) using BS3 (Thermo Scientific, 5 mM in 20 mM sodium phosphate, 150 mM NaCl, pH 8) rotating for 30 min at room temperature and quenched by addition of 50 mM Tris-HCl pH 7.5 rotating for 15 min at room temperature. Beads were then incubated with lysates on a rotating wheel for 2 h at 4°C, magnetically isolated, washed and analyzed by SDS-PAGE and immunoblotting using rabbit anti nidogen-2 (Abcam, ab14513; 1:500) and rat anti HA (3F10, Roche; 1:1000) antibodies.

Molecular modelling of the nidogen-1/N1 peptide-H_CT interaction

The crystal structure of H_CT with the tri-peptide YEW bound (PDB ID 1YXW)(*6*) was used as a template. The N1 peptide (THIYQWRQT) was built using software Coot (*30*) replacing the glutamic acid with a glutamine within the YEW peptide; the remaining residues (THI---RQT) were manually built and adjusted inside the crevice of H_CT. The structure was optimized by several runs of energy minimisation with the CNS software (*31*).

A model of the human nidogen-1 fragment (amino acids 389 to 661), was built by homology modeling using the Swiss-Model web server (*32*) based on the crystal structure of mouse nidogen-1 G2/perlecan Ig3 complex as a template (PDB code 1GL4) (*33*). There is 85% sequence identity between the human and mouse proteins.

The peptide 604-612 of human nidogen-1 was manually superimposed to N1 peptide in the nidogen-1-H_CT complex using Coot. The model of the two proteins was optimized by energy minimisation and subjected to molecular dynamics with software CNS. Several steps of dynamics at room temperature were performed, keeping the structure of nidogen-1 fixed. The Cα atoms of H_CT were harmonically restrained during the dynamics, with the exception of residues 1142-1149 and 1212-1227 in the interaction region of the two proteins, which were left free to move.

Immunofluorescence assays on primary motor neurons

Spinal cord motor neurons were prepared from E13.5 old mouse embryos (C57/Bl6, Charles River) and plated onto poly-L-ornithine and laminin coated glass coverslips, or microfluidic chambers (*21*). For H_CT binding studies, wild type motor neurons were cooled on ice prior to incubation with H_CT (20 nM), which was pre-treated with either DMSO, or the N1/$N1_{AA}$ peptide (20 µM), or recombinant nidogens (1 nM), or a combination of the above for 1 h at room temperature at a molar ratio of 1:20:20,000 (recombinant nidogen-1:H_CT:N1/$N1_{AA}$ peptide). Cells were incubated with fluorescent H_CT for 10 min before washing with ice-cold Hanks' buffer (20 nM HEPES-NaOH pH 7.4, 0.44 mM KH_2PO_4 0.42 mM NaH_2PO_4, 5.36 mM KCl, 136 mM NaCl, 0.81 mM $MgSO_4$, 1.26 mM $CaCl_2$, 6.1 mM glucose) and fixing with 4% paraformaldehyde (PFA) in PBS for 15 min at room temperature. To obtain a mask for fluorescence intensity quantification, we stained the cells with a mouse monoclonal antibody against βIII tubulin (Covance, MMS-435P; 1:1,000) and an AlexaFluor488-conjugated goat anti-mouse secondary antibody (1:500). Twenty images were acquired for each condition using a Zeiss LSM510 confocal microscope equipped with a Zeiss 40x objective and analyzed for H_CT binding using Cell Profiler. The mean fluorescence intensity was plotted for each condition and statistical significance was analyzed using one-way ANOVA followed by Dunnett's multiple comparison test.

For assessing the ability of nidogen-2 KO primary motor neurons to bind H_CT, we isolated motor neurons from nidogen-2 KO and wild type embryos and cultured them for 7-10 days (DIV 7-10). Cells were cooled on ice, and incubated with H_CT (20 nM) for 10 min. Following a wash with ice-cold Hanks' buffer, the cells were fixed with 4% PFA in PBS for 15 min at room temperature). We stained the coverslips with mouse monoclonal antibody against βIII tubulin (Covance, MMS-435P; 1:1,000) and an AlexaFluor488-conjugated goat anti-mouse secondary antibody (1:500). Ten images were acquired for each condition using a Zeiss LSM510 confocal microscope equipped with a Zeiss 40x objective and analyzed for H_CT binding using Cell Profiler. The mean fluorescence intensity was plotted for each genotype and statistical significance was analyzed using unpaired t test with Welch's correction.

For co-localization studies, motor neurons were incubated with fluorescent H_CT (40 nM) together with rabbit polyclonal antibody against nidogen-2 (Abcam, ab14513; 1:500) at 37°C for 45 min, then cooled on ice and subjected to an acid wash (2 min; 100 mM citrate-NaOH, 140 mM NaCl, pH 2.0) to remove the surface bound probes before fixation with 4% PFA in PBS for 15 min at room temperature. Cells were permeabilized using 0.1% Triton X100 in PBS for 10 min at room temperature and blocked with 5% BSA in PBS for 1 h. The primary antibody was revealed using an AlexaFluor647 goat-anti-rabbit secondary antibody.

For the SV2 co-localization studies, motor neurons were incubated either with fluorescent H_CT alone (40 nM), or together with recombinant nidogen-1 (1.6 nM; R&D Systems; 2570-ND-050) for 45 min at 37 °C. Cells were then acid washed, fixed, permeabilized and blocked as described above prior to staining with a rabbit polyclonal antibody against SV2A (Synaptic System; SYSY119002; 1:500) or SV2C (a kind gift by T. Südhof; 1:100) and a mouse monoclonal antibody against βIII tubulin. Primary antibodies were detected as described above.

Samples were imaged as before using a Zeiss 63x, Plan Apochromat oil-immersion objective. The Zeiss LSM510 confocal microscope was optimized for co-localization analysis and the pinholes were adjusted to match each other in every channel. The sampling was set to maximum and the level of co-localization was quantified using ImageJ. We determined Mander's coefficient on randomly chosen fields and statistical significance was assessed using unpaired t test with Welch's correction.

For transcytosis assays, we designed microfluidic chambers with short microgrooves (500 μm). Chambers were hydrated with 0.8% BSA in PBS overnight at 37°C before coating with poly-L-ornithine and laminin (*21*). Primary motor neurons were plated in the somatic side (CB; Supplementary Fig. 3a) and left to adhere before adding filling the chamber with complete motor neuron medium. Experiments were performed between DIV7-10 after the neurons have extended their axons to the other side of the chamber.

To test whether nidogen-2 was re-exposed together with H_CT on the surface of motor neurons after axonal retrograde transport, we added AlexaFluor555-HA-H_CT (40 nM) together with a rabbit polyclonal antibody against nidogen-2 (Abcam; ab14513; 1:500) to the axonal side (AX; Supplementary Fig. 3a) of the device and incubated for 2 h at 37°C. Cells were then fixed with 4% PFA in PBS, blocked with 5% BSA in PBS and stained with

a monoclonal anti-HA antibody (Roche; 3F10; 1:500) in detergent-free conditions. Samples were washed and stained with goat anti-rabbit (AlexaFluor647; 1:500) and anti-mouse (AlexaFluor488) secondary antibodies (1:500) to reveal the transcytosed pool of H_CT and nidogen-2, respectively.

Hemidiaphragm and muscle tissue preparation

Mouse phrenic nerve-hemidiaphragms were dissociated from male Swiss-Webster CD1 mice weighting about 20 g and mounted in 2-4 ml of oxygenated (95% O_2, 5% CO_2) Krebs-Ringer solution of the following composition: 137 mM NaCl, 5 mM KCl, 1.8 mM $CaCl_2$, 1.0 mM $MgCl_2$, 24 mM $NaHCO_3$, 1 mM NaH_2PO_4 and 11 mM glucose, pH 7.4, at 37°C. Two innervated hemidiaphragm preparations were isolated from each animal; muscles were stretched to the optimal length for twitch response and allowed to equilibrate for at least 20 min at 37°C before the start of the experiment. The phrenic nerve was stimulated via two ring platinum electrodes with supramaximal stimuli of 10 V amplitude and 0.1 ms pulse duration with a frequency of 0.1 Hz. Muscle contraction was monitored with an isometric transducer (Harvard Apparatus); data was recorded and analyzed via an i-WORX 118 system with Labscribe software (Harvard Apparatus). TeNT aliquots (final concentration 5 nM) were preincubated with vehicle (DMSO) or with the N1 peptide (2.5 μM), corresponding to a molar ratio of 1:500 (TeNT:peptide), for 1 h at room temperature, and then added directly to tissue bath of two nerve-muscle preparations obtained from a single animal. Muscular twitch was monitored until complete paralysis. Data are expressed as time required to decrease the twitch to 50% of the initial value (paralysis half-time).

To determine whether nidogen-2 and H_CT co-localize at the NMJ, we isolated *levator auris longus* (LAL) muscles from wild type mice and incubated them with H_CT (40 nM) and the rabbit antibody against nidogen-2 (1:500) in motor neuron medium. The muscle was then fixed in 10% neutral buffered formalin (NBF) overnight at 4°C, then permeabilized and blocked using 1% BSA and 0.1% Triton-X100 in PBS for 2 h at room temperature. A rat anti-HA antibody (3F10, Roche; 1:1,000) was added to the sample. Following washing with PBS, samples were stained with goat secondary antibodies against rabbit (AlexaFluor647) and rat (AlexaFluor488) IgG (1:500), and with AlexaFluor555-αBTX (1:1,000), mounted with Mowiol and imaged using a Zeiss LSM780 confocal microscope equipped with a Zeiss 40x Plan Apochromat oil-immersion objective.

We isolated LAL muscles from nidogen-2 KO mice to assess their ability to accumulate H_CT at the NMJ. The muscles were incubated with H_CT (20 nM) in motor neuron medium for 2 h at 37 °C, fixed in 10% NBF overnight at 4°C then subjected to the same immunofluorescence protocol as before. We used AlexaFluor555-BTX (1:1,000) and goat α-rat AlexaFluor488-IgG (1:500), to identify the NMJs and assess H_CT binding. The muscles were mounted with Mowiol and imaged using a Zeiss LSM780 confocal microscope equipped with a Zeiss 40x Plan Apochromat oil-immersion objective. We used BTX staining as a mask and analyzed H_CT binding by measuring the mean fluorescence intensity of the green channel in Cell Profiler. The results were plotted and tested for significance by one-way ANOVA followed by Dunnett's multiple comparison test.

We dissected hindbrains of nidogen-1 and -2 KO (DKO) embryos at E11.5 to determine whether the complete loss of nidogens affects H_CT binding. The hindbrain preparations were incubated with H_CT in motor neuron medium for 2 h at 37 °C, followed

by 10% NBF fixation overnight at 4°C. The samples were immunostained using the same protocol as for the nidogen-2 KO motor neurons. The hindbrains were mounted with Mowiol and imaged using a Zeiss LSM780 confocal microscope equipped with a Zeiss 20x Plan Apochromat objective. The mean grey value of the red channel was determined within the boundaries of the hindbrain in Image J, plotted and tested for significance using unpaired t test.

Footprint and gait analysis

Age and body mass matched C57/Bl6 male mice were injected with TeNT (1 or 2 ng/kg) preincubated with either DMSO, the N1 or the $N1_{AA}$ peptide at a molar ratio of 1: 13,800 (TeNT:peptide) for 1 h at room temperature at two different doses in the right *triceps surae* muscle. Mice were monitored for period of 96 h unless they reached the humane endpoint (appearance of moderate symptoms: hunched back and paralysis of rear limbs, or disappearance of the righting reflex for 30 s) earlier. We performed a footprint assay as previously described (*34*). To quantify the extent of paralysis, we measured the distance between the contralateral (injected side) front and hind paw prints. This parameter provides a reliable assessment of normal foot positioning during walking in mice, whereas *triceps surae* paralysis results in an increased distance between. Data were analyzed using one-way ANOVA followed by Dunnett's multiple comparison test to compare the groups. Following termination, *triceps surae* muscles were dissected and weighed to determine whether the administered dose based on total body weight was in accordance with the dose/mg muscle.

Isometric muscle tension physiology

8-week old female C57Bl6 mice received unilateral intramuscular injection into the *tibialis anterior* (TA) muscle of TeNT (0.125 ng/kg, 4 µl total volume per 20 g body mass), after preincubation with vehicle (DMSO), N1 or $N1_{AA}$ peptides at a molar ratio of 1: 13,800 (TeNT:peptide) for 1 h at room temperature. After 24 h, under terminal anaesthesia, isometric muscle tension force was recorded from the distal TA tendon following electrical stimulation (40-100 Hz, 0.02 ms square-wave pulses, for 450 ms) of the exposed sciatic nerve to induce maximal tetanic muscle contraction, as previously described (*35*). Contractile force of injected muscles was compared to contralateral (non-injected) TA muscle, as an internal control, and average changes within each group were analyzed using unpaired t test.

Analysis of TeNT toxicity in nidogen-2 KO mice

Age and body mass-matched wild type and nidogen-2 KO mice were injected intraperitoneally with different doses of TeNT (1.5, 3, 6, 12 ng/kg). Mice were monitored for up to 96 h. The experiment was terminated when mice showed moderate symptoms (hunched back and paralysis of rear limbs or disappearance of the righting reflex for 30 s). The time of survival prior to termination was plotted against the administered dose of TeNT. The groups were analyzed using paired t test for each dose.

Supplementary Tables and Figures

Peptide	Gene name	Sequence
A	Coxsackievirus and adenovirus receptor homolog	PLQFEWQKL
B	Glypican-4	DLDFEWNNF
C	Neural cell adhesion molecule 1	VAVYTWEGN
D	**Nicastrin**	**SRSFFWNVA**
D_A	Nicastrin	SRSFFANVA
D_{AA}	Nicastrin	SRSAFANVA
D2	**Nicastrin**	**SRSFFWNVA**
D3	Nicastrin	LYEYSWVQG
E	Poliovirus receptor-related protein 2/Nectin-2	PTDYDWSTT
E2	Poliovirus receptor-related protein 2/Nectin-3	PTDAAASTT
F	Msn	KIGFPWSEI
G	Sodium/potassium-transporting ATPase subunit a1	ILEYTWLEA
H	Sodium/potassium-transporting ATPase subunit a3	ILGYTWLEA
I	Voltage-dependent calcium channel subunit a2/d1	NRTYTWTPV
J	**Vdac3 voltage gated anion channel**	**PTIYGWAVL**
J_{AA}	Vdac3 voltage gated anion channel	PTIAGAAVL
K	Voltage-dependent anion-selective channel protein 1	ETKYRWTEY
L	Voltage-dependent anion-selective channel protein 2	ETKYKWCEY
N1	**nidogen-1**	**THIYQWRQT**
$N1_{AA}$	nidogen-1	THIAQARQT
N_4	nidogen-1	STGYCWCVD
N3	**nidogen-1**	**LVGFLWKSN**
$N3_{AA}$	nidogen-1	LVGALAKSN
O	**Lysosome membrane protein 2**	**GLIFTWLAC**
P	Putative phospholipase B-like 2	CPPFQWSKS
R	St13 Hsc70-interacting protein	AQPYKWRGK
SV2A	SV2A	IPHYGWSFQ
SV2B	SV2B	IPHYGWGFS
SV2C	SV2C	IPHYGWSFS
$ND3_{-1}$	nidogen-2	GGLFGWLFA
$ND3_{-2}$	nidogen-2	STGFCWCVD
$ND3_{-3}$	nidogen-2	KSDFCWCVD
N2	**nidogen-2**	**NQTWSYHID**
$N2_{AA}$	nidogen-2	NQTASAHID
$ND3_{-5}$	nidogen-2	KEFYHYRDS

Supplementary Data Table 1.
Components of signalling endosomes containing variants of the YEW motif. The sequences of the nine-residue peptides containing these motifs, which were identified in the proteome of H_CT-positive axonal signalling endosomes, are shown on the right, whilst unique identifiers for each peptide are shown on the left. These peptides were tagged with biotin and HPLC-purified before further analyses. Peptides that showed detectable binding

in at least one of the assays shown in Fig. 1a and Supplementary data Fig. 2 are in bold, and the N1 (nidogen-1) and N2 (nidogen-2) peptides are in red.

Bond	H_CT	Distance (Å)	nidogen-1 (N1 peptide)
H-bond			
1	A:ASP1214[OD2]	2.81	P:THR1[OG1]
2	A:ARG1226[NE]	3.47	P:GLN5[OE1]
3	A:LYS1143[NZ]	2.91	P:GLN8[OE1]
4	A:LYS1143[NZ]	3.22	P:GLN8[O]
5	A:ASP1278[OD1]	3.08	P:GLN8[NE2]
Polar			
6	A:ILE1224[O]	Via a water molecule	P:GLN5[OE1]
7	A:LYS1213[O]	Via a water molecule	P:ILE3[O]
8	A:GLY1233[O]	3.15	P:HIS2[ND1]

Supplementary Data Table 2.
Potential hydrogen bonds and other polar interactions between H_CT (A) and the N1 peptide from nidogen-1 (P). The predicted distance between the interacting residues is indicated. Distances must be considered as indicative, since they are based on a theoretical model. Contacts and concealed surfaces were calculated with server PISA (http://www.ebi.ac.uk).

Bond	H_CT	Distance (Å)	nidogen-1 (G2 domain)
1	A:ASN1144[ND2]	2.64	D:HIS 575[O]
2	A:ASN1144[ND2]	2.85	D:VAL 580[O]
3	A:THR1146[OG1]	3.48	D:THR 582[O]
4	A:ASN1216[ND2]	3.67	D:GLU 521[OE2]
5	A:TYR1229[OH]	2.91	D:SER 584[OG]
6	A:ASN1277[N]	2.63	D:THR 614[OG1]
7	A:ASN1277[ND2]	3.83	D:THR 614[O]
8	A:ILE1145[O]	3.85	D:THR 582[OG1]
9	A:LYS1213[O]	3.88	D:THR 586[OG1]
10	A:ASP1214[O]	2.82	D:ARG 610[NH1]

11	A:GLY1215[O]	2.71	D:ARG 610[NH2]
12	A:GLY1215[O]	3.56	D:THR 523[OG1]
13	A:ALA1217[O]	3.06	D:ASN 530[ND2]
14	A:TYR1229[OH]	3.74	D:THR 586[N]
15	A:TYR1229[OH]	2.94	D:GLN 608[NE2]

Supplementary Data Table 3.
Potential hydrogen bonds between H_CT (A) and the G2 domain of nidogen-1 (D). The predicted distance between the interacting residues of H_CT (A) and the intact G2 domain of nidogen-1 (D) is indicated. Distances must be considered as indicative, since they are based on a theoretical model. Contacts and concealed surfaces were calculated as described in Supplementary Data Table 2.

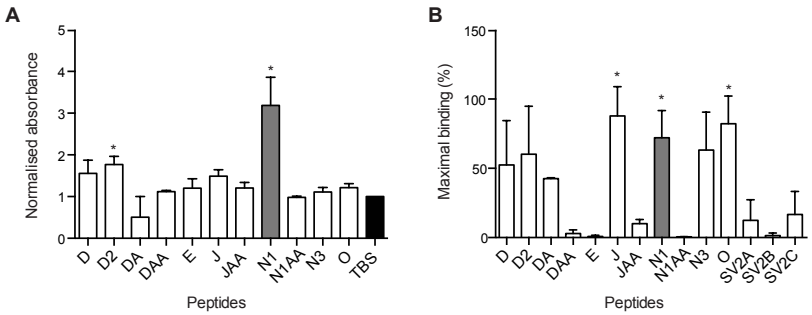

Supplementary Fig. 1.
The N1 peptide binds to H_CT in ELISA and immunoprecipitation assays. (A) Selected peptides (see Supplementary Data Table 1) were dried on 96-well plates, blocked for non–specific binding and incubated with VSVG-tagged H_CT, which was detected by ELISA at 490 nm using Tris-buffered saline (TBS) as a control. Statistical significance was tested using paired t test (n=3; *, $p<0.05$; error bars: SD). **(B)** Selected biotin-tagged peptides containing variants of the YEW motif and their alanine mutants were bound to streptavidin beads and incubated with recombinant VSVG-tagged H_CT. After washing, the captured H_CT was eluted from the beads, subjected to SDS-PAGE and detected by western blotting. Band intensity was determined by densitometry using ImageJ. The results were normalized to empty beads control and analyzed using paired t test (n=3 for wild type peptides, n=2 for mutants; *, $p<0.05$; error bars: SD).

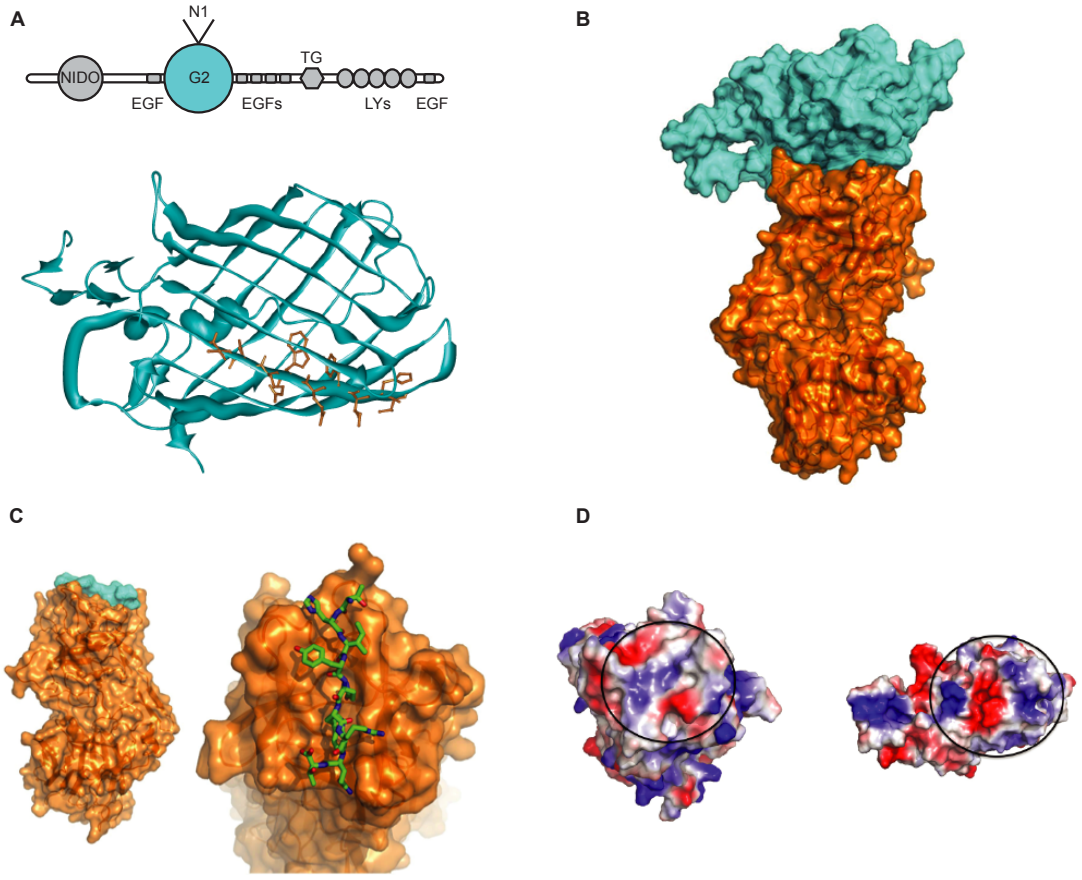

Supplementary Fig. 2.
Molecular modelling of H_CT-N1 peptide and H_CT-nidogen-1 G2 domain interactions. **(A)** Module structure of nidogen-1 showing the position of the N1 peptide within the b-barrel G2 domain (cyan; top). In addition to the G2 domain, nidogen-1 contains a nidogen domain (NIDO), six EGF-like domains (EGFs), a thyroglobulin type 1 domain (TG) and five low-density lipoprotein receptor (LY) domains. Crystal structure of nidogen-1 G2 domain (cyan; bottom) with the stick model of the N1 peptide (orange; bottom, PDB ID: 1h4u(*36*). **(B)** Model of the complex of G2 domain of human nidogen-1 (cyan) and H_CT (orange). The G2 domain was manually superimposed to the N1 peptide, using the graphic program Coot (*30*). **(C)** Details of the crystal structure of H_CT (orange) bound to peptide N1 (stick model; PDB code 1XYW(*6*)). The N1 peptide was built using Coot, the glutamic acid of the YEW sequence present in the PDB structure 1XYW(*6*) was replaced with a glutamine; the remaining residues (THI---RQT) were manually built and adjusted inside the crevice of the toxin. The surface concealed by the formation of the N1 peptide-H_CT complex is 518 $Å^2$ for the H_CT domain and 592 $Å^2$ for the N1 peptide. This site is located on the opposite side of the main binding domain for polysialogangliosides, which have an established role as clostridial neurotoxin co-receptors (*18*), and should not interfere with ganglioside binding. **(D)** Qualitative electrostatic potential surface of interacting regions of H_CT (left) and the nidogen-1 G2 domain (right). Circles highlight the two interacting areas, which are predicted to be complementary in terms of electrostatic charges. The bottom of

the H_CT crevice is slightly positively charged, whilst the two borders are mostly negative; in contrast, the central area of the interacting surface of nidogen-1 is negatively charged, whilst the borders are positive.

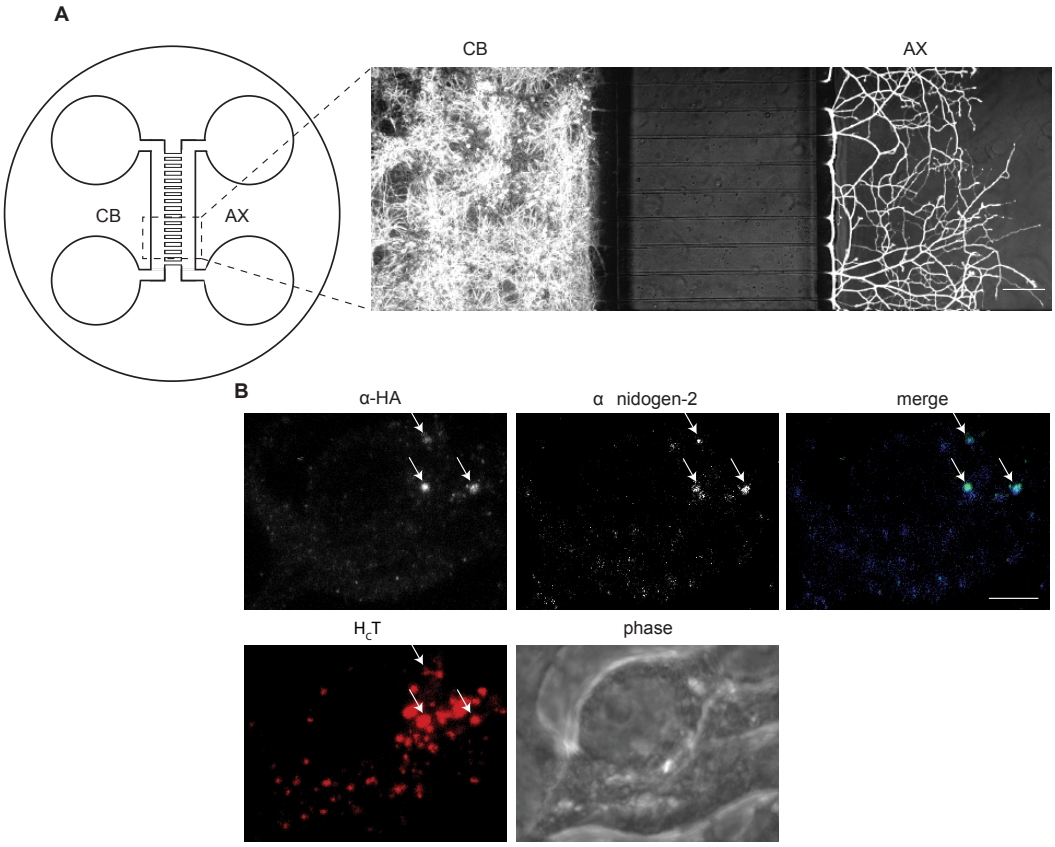

Supplementary Fig. 3.
Nidogen-2 and H_CT undergo transcytosis in primary motor neurons grown in microfluidic chambers. (A) Primary motor neurons were plated into the somal side (CB) of microfluidic chambers, and both CB and axonal (AX) compartments were stained with anti βIII tubulin antibodies to show that motor neuron axons crossed the microgrooves. Scale bar, 100 μm. **(B)** AlexaFluor555-HA-H_CT (bottom left) and an antibody against nidogen-2 (a nidogen-2) were added to the AX compartment of microfluidic chambers containing primary motor neurons and incubated for 2 h at 37˚C. This allows for uptake, axonal retrograde transport and transcytosis of H_CT and nidogen-2 in the CB compartment. Cell surface staining of axonally-derived, transcytosed AlexaFluor555-HA-H_CT using an anti-HA antibody is on the top left panel. An anti-rabbit AlexaFluor647 secondary antibody was used to detect the transcytosed a nidogen-2 (top, middle panel). Both surface-exposed H_CT (in green) and nidogen-2 (in blue) are transcytosed together under these conditions (merge, arrows; top right panel). The somatic distribution of the total AlexaFluor555-HA-H_CT, which underwent axonal retrograde transport, is shown on the bottom left panel (in red). Scale bar, 5 μm.

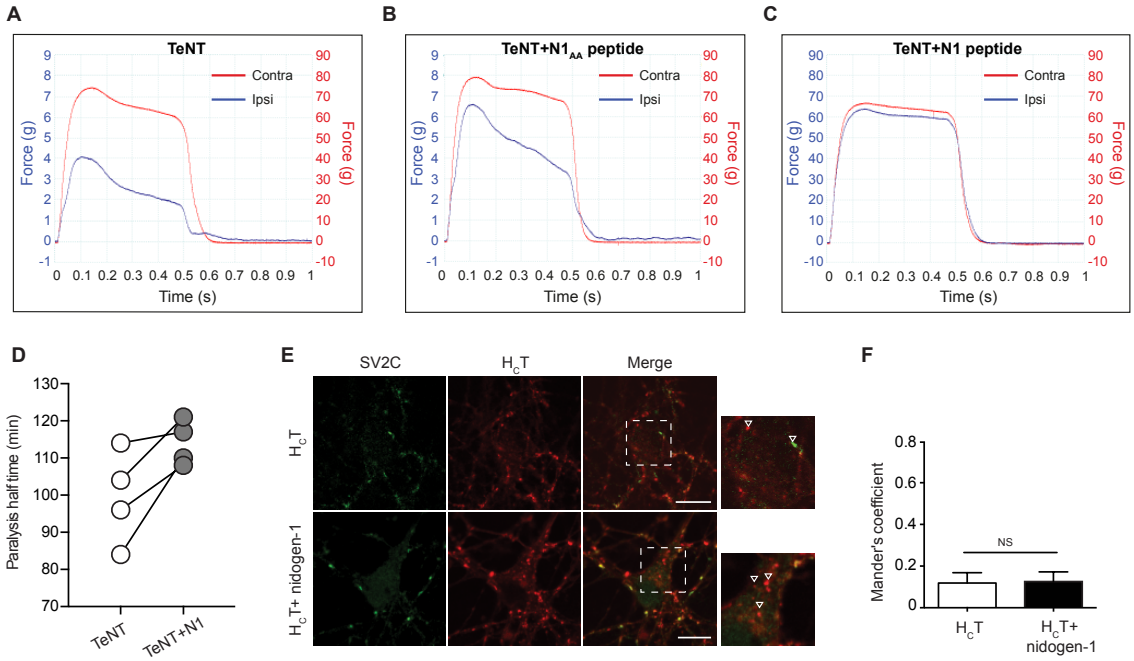

Supplementary Fig. 4.

The N1 peptide of nidogen-1 delays TeNT paralysis both in the TA muscle and in the phrenic nerve-hemidiaphragm preparation. (A-C) Representative isometric muscle force recordings obtained from the ipsilateral (ipsi; injected side) and contralateral (contra; non-injected internal control) *tibialis anterior* muscles, 24 h after administration of TeNT preincubated with vehicle control (DMSO) **(A),** or the $N1_{AA}$ peptide **(B)** or the N1 peptide (**c**). Ten fold lower scale was applied to ipsilateral and contralateral traces in **(A)** and **(B)**, while the scales are identical for both traces in **(C)** (*n*=6 mice per group). **(D)** TeNT preincubated with vehicle (DMSO) or the N1 peptide was added to the nerve-muscle preparations in Krebs-Ringer solution at 37°C. Muscle twitch was induced by nerve stimulation and paralysis times were monitored. Data is expressed as paralysis half time and reported as paired observations (*n*=4). **(E)** Wild type motor neurons were incubated either with AlexaFluor555-H_CT (shown in red; 40 nM) alone, or together with full length nidogen-1 (1.3 nM) for 45 min at 37 °C. Cells were washed, fixed and immunostained for SV2C (shown in green) and βIII tubulin (not shown). **(F)** Mander's coefficient was used to quantify the extent of co-localization. Significance was assessed by unpaired t test (*n*=3, 10 images per experiment; NS, non significant; error bar: SD). Scale bar, 10 µm.

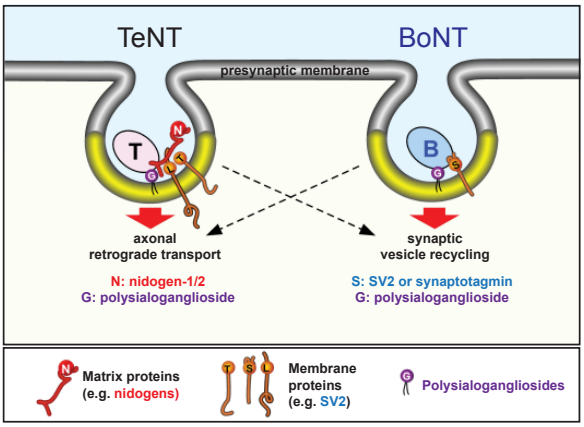

Supplementary Fig. 5.
Cross-talk between the uptake and trafficking routes of TeNT and BoNTs. At physiological concentrations, TeNT and BoNT enter motor neurons using trafficking pathways that are mutually exclusive: BoNTs are mainly internalised by the synaptic vesicle recycling pathway, whereas TeNT is taken up by a clathrin-dependent route linked to axonal retrograde transport. Specific protein receptors zed on synaptic vesicles and exposed during synaptic activity (e.g. SV2A-C, synaptotagmin I and II) or at specialised entry sites of the NMJ (nidogens), direct these neurotoxins to different intracellular organelles. However, high concentrations of either TeNT or BoNTs alter this equilibrium resulting in crosstalk between their respective entry routes (arrows). Addition of exogenous recombinant nidogens, which would not be expected to be fully sequestered into the extracellular matrix, enhances H_CT binding to motor neurons and reduces the co-localization with SV2A. This model suggests that in the presence of nidogens, H_CT is preferentially directed towards a cellular entry route linked to axonal retrograde transport and transcytosis in motor neurons, which is ultimately responsible for the targeting of TeNT to the spinal cord and the characteristic spastic paralysis of tetanus.

Supplementary Movie 1.
Mice injected in the right *triceps surae* muscle with TeNT showed signs of local paralysis (the affected limb is extended) with no grip reflex. Pre-treatment of TeNT with vehicle control or the $N1_{AA}$ peptide had no effect on the progression of tetanic paralysis. In contrast, when mice were injected with TeNT pre-treated with the N1 peptide, they showed an overall normal posture, strong grip reflex and no gait abnormalities, demonstrating a blockade in TeNT-induced paralysis.